Critical-angle transmission grating spectrometer for high-resolution soft x-ray spectroscopy on the International X-ray Observatory

Ralf K. Heilmann,[a] John E. Davis,[a] Daniel Dewey,[a] Mark W. Bautz,[a] Rick Foster,[a] Alex Bruccoleri,[a] Pran Mukherjee,[a] David Robinson,[b] David P. Huenemoerder,[a] Herman L. Marshall,[a] Mark L. Schattenburg,[a] Norbert S. Schulz,[a] L. Jay Guo,[c] Alex F. Kaplan,[c] Russell B. Schweikart[d]

[a]MIT Kavli Institute for Astrophysics and Space Research,
Massachusetts Institute of Technology, Cambridge, Massachusetts 02139, USA
[b] NASA Goddard Space Flight Center, Greenbelt, MD 20771, USA
[c] University of Michigan, Ann Arbor, MI 48109, USA
[d] Ball Aerospace & Technologies Corp, 1600 Commerce St., Boulder CO 80301

ABSTRACT

High-resolution spectroscopy at energies below 1 keV covers the lines of C, N, O, Ne and Fe ions, and is central to studies of the Interstellar Medium, the Warm Hot Intergalactic Medium, warm absorption and outflows in Active Galactic Nuclei, coronal emission from stars, etc. The large collecting area, long focal length, and 5 arcsecond half power diameter telescope point-spread function of the International X-ray Observatory will present unprecedented opportunity for a grating spectrometer to address these areas at the forefront of astronomy and astrophysics. We present the current status of a transmission grating spectrometer based on recently developed high-efficiency critical-angle transmission (CAT) gratings that combine the traditional advantages of blazed reflection and transmission gratings. The optical design places light-weight grating arrays close to the telescope mirrors, which maximizes dispersion distance and thus spectral resolution and minimizes demands on mirror performance. It merges features from the Chandra High Energy Transmission Grating Spectrometer and the XMM-Newton Reflection Grating Spectrometer, and provides resolving power $R = E/\Delta E = 3000 - 5000$ (full width half max) and effective area > 1000 cm^2 in the soft x-ray band. We discuss recent results on ray-tracing and optimization of the optical design, instrument configuration studies, and grating fabrication.

Keywords: x-ray optics, International X-ray Observatory, IXO, critical-angle transmission grating, x-ray spectroscopy, blazed transmission grating, sub-aperture, soft x-ray, ray tracing

1. INTRODUCTION

As often stated by those skilled in the art, "spectroscopy puts the 'physics' into astrophysics". For x-ray energies below a few keV spectroscopic data from celestial sources with resolving power up to $R = E/\Delta E = 1500$ as delivered by the Chandra High-Energy Transmission Grating Spectrometer (HETGS)[1] have provided copious amounts of new information and have lead to many exciting discoveries during the last decade. A wealth of new knowledge - of course accompanied by many new questions - has been gathered on young stars, supernova remnants, neutron stars, small and super massive black holes, highly energetic jets, etc. However, for most energies the resolving power is well below $R = 1000$, the effective area is below 100 cm^2, and an increasing number of observations that are trying to push the envelope of our knowledge is hampered by these factors. The International X-Ray Observatory (IXO)[2] - a joint NASA, ESA, and JAXA effort - is designed to improve upon this situation by more than an order of magnitude. High spectral resolution, high effective area spectroscopy for keV photons will be enabled by an energy dispersive microcalorimeter array at the focus of a 20 m focal length

Further author information: Send correspondence to R.K.H. E-mail: ralf@space.mit.edu, URL: http://snl.mit.edu/home/ralf

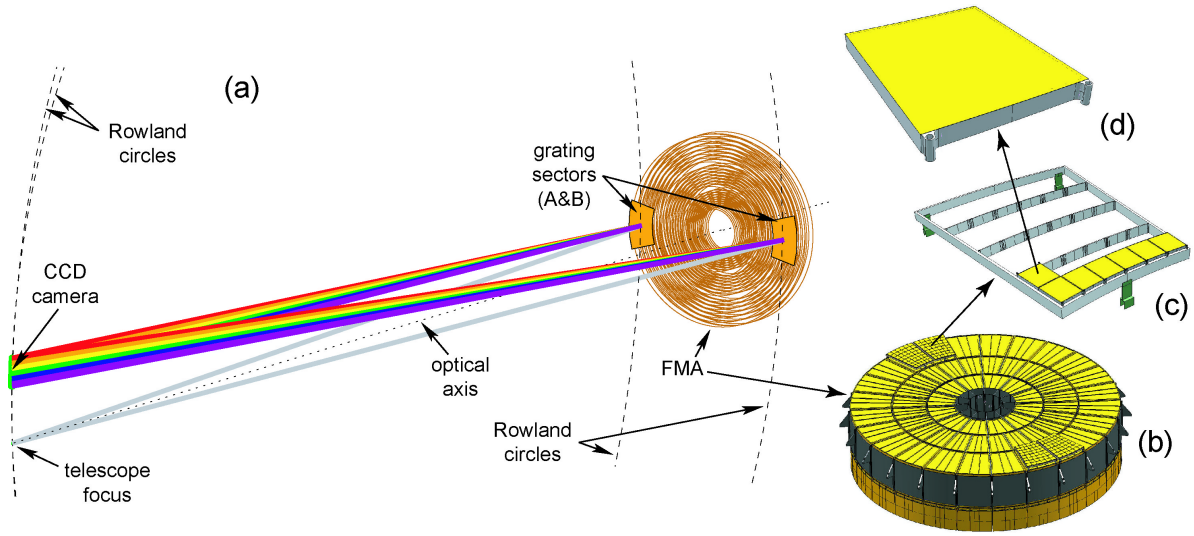

Figure 1. Schematic of CAT grating spectrometer and structural hierarchy of grating arrays. (a) Perspective view of telescope optics covered by two grating sectors and representative paths of transmitted x rays. (b) Model of ~ 3.2 m diameter slumped glass flight mirror assembly (FMA) with four grating array structures (GAS). (c) Single GAS, partially populated with grating facets. (d) Grating facet, consisting of a thin metal grating frame and a monolithic silicon membrane that contains the CAT gratings and two levels of support structure.

telescope with ~ 3 m^2 effective area and 5 arcsec (half power diameter - HPD) angular resolution. At lower energies higher spectral resolution can be achieved via wavelength dispersion with an x-ray grating spectrometer (XGS). The XGS science performance requirements are $R = E/\Delta E > 3000$ and effective area > 1000 cm^2 for point sources over the soft x-ray band of 0.3 to 1.0 keV.

The science case for a soft x-ray spectrometer on IXO has been made in numerous papers,[3] ranging from detection of the warm/hot intergalactic medium (WHIM) and detection of flows in the galactic and intergalactic media, to studies of gas and dust in the Interstellar Medium and of emission anomalies in the spectra of young stars.

In the following we describe and present the status of a blazed x-ray transmission grating spectrometer[4,5] that meets and exceeds the IXO XGS science requirements. It features recently developed high-efficiency, lightweight, alignment, figure and polarization insensitive critical-angle transmission (CAT) gratings[5–7] and an order-sorting camera consisting of a linear CCD array that is laterally displaced from the telescope focus and operates simultaneously with the focal plane detector of choice (X-ray Microcalorimeter Spectrometer, Wide Field Imager, Hard X-ray Imager, High Time Resolution Spectrometer, X-ray Polarimeter). An added benefit of the CAT gratings is that they are highly transparent at higher energies and thus their zeroth order transmission contributes to the effective area at the imaging focus.

Below we shall first describe the optical design of the CAT grating spectrometer (CATGS), then discuss recent ray trace results and their implications on spectral resolution, followed by an update on configuration studies and recent grating fabrication results.

2. CAT GRATING SPECTROMETER (CATGS) DESIGN

The optical and mechanical design of the CATGS is similar to the design for the Chandra HETGS,[1] but modified due to the blazing capability of the CAT gratings (see Fig. 1). A part of the IXO mirror aperture is covered by an array of transmission grating elements. We refer to these elements as grating facets. Each facet consists of a thin, highly structured silicon membrane up to 60×60 mm in size and contains free-standing CAT gratings. Each membrane is supported by a narrow frame, which in turn is mounted to a Grating Array Structure (GAS). There are two to four GAS's, depending on the layout of the 20m-focal-length telescope Flight Mirror Assembly

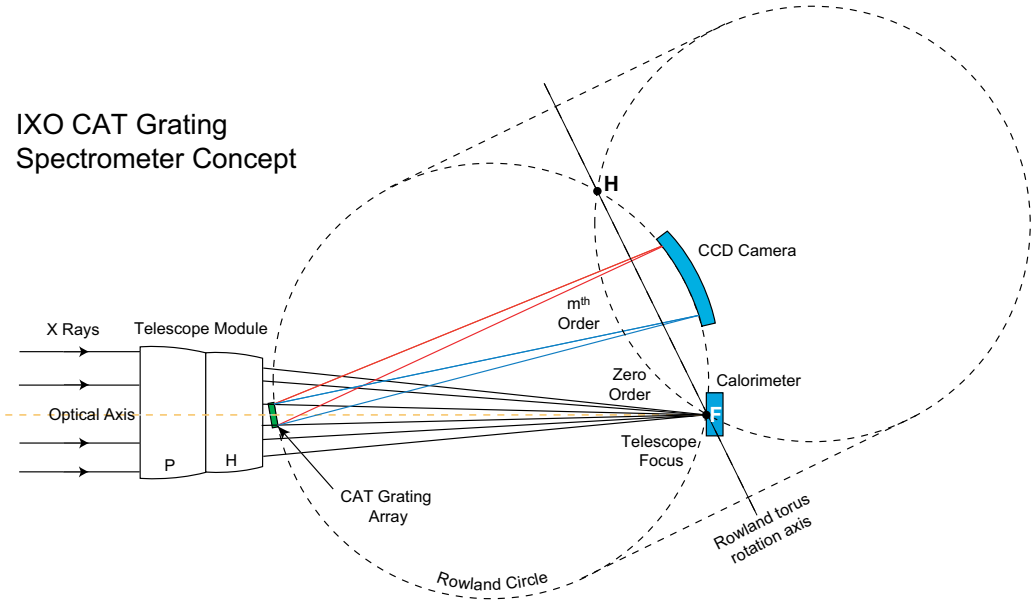

Figure 2. Schematic of CAT grating spectrometer optical design (not to scale). X rays are focused by the parabolic (P) and hyperbolic (H) mirror shells of the segmented Wolter-I optic on the point F. CAT gratings intercept a fraction of the x rays and diffract them predominantly at angles centered around the blaze direction. Representative paths for longer (red) and shorter (blue) wavelength rays diffracted in m^{th} order are shown. See text for more detail.

(FMA). Each GAS is densely populated with grating facets and placed into the converging telescope beam just downstream of the FMA. The resulting grating arrays form two azimuthally juxtaposed grating sectors A and B, each sector covering slightly less than 30 degrees in azimuth. Radial coverage starts from the outermost mirrors (radius > 1.5 m) and ends towards smaller radii as soon as the effective area requirements are met.

Placement of the grating facets and the readout camera is governed by a Rowland torus geometry[1,5] and the blaze angle of the CAT gratings, chosen at $2 \times 1.5°$. The Rowland torus is generated by rotating a circle that contains the telescope focus F around an axis that contains the focus and a second point H on the circle (see Fig. 2). We refer to these two points as "hinges". The radius of the circle is chosen to place the gratings as far as possible away from the focus. Of course placing the gratings at maximum distance from focus generates the maximum possible dispersion distance, which in turn serves to obtain the maximum possible spectral resolution. This is a very important point, as we will see below. Another factor in the choice of torus parameter is the fact that each CAT grating facet is oriented with its normal 1.5° from the incident "on-axis" ray that hits its center. Since the facet is flat it cannot conform to the Rowland torus surface, which leads to aberrations that grow with the size of the facet. On Chandra the optical axis of the telescope intersects the center of the circle and x rays are normal to the facet surfaces. For the CATGS we chose to shift the center of the circle away from the optical axis towards the blaze direction, and to simultaneously increase its radius (see Fig. 2). This change from the previously described design[5] allows us to minimize grating facet deviations from the torus surface and resulting aberrations. Due to blazing it also is advantageous to choose the second hinge in the general proximity of the blaze condition. Not surprisingly this results in a Rowland torus geometry very similar to that of the blazed Reflection Grating Spectrometer (RGS) on XMM-Newton.[8] The exact choice of the second hinge position has a negligible effect on resolution in the dispersion direction, but a pronounced effect on astigmatism. We have currently settled on a design that places the second hinge at an angle of 6 degrees from the optical axis. This has the advantage that the two grating sectors generate two spatially separated spectra and greatly relaxes relative alignment tolerances between the two sectors. It also allows one to think about populating the two grating sectors with two different types of CAT gratings with complementary properties.

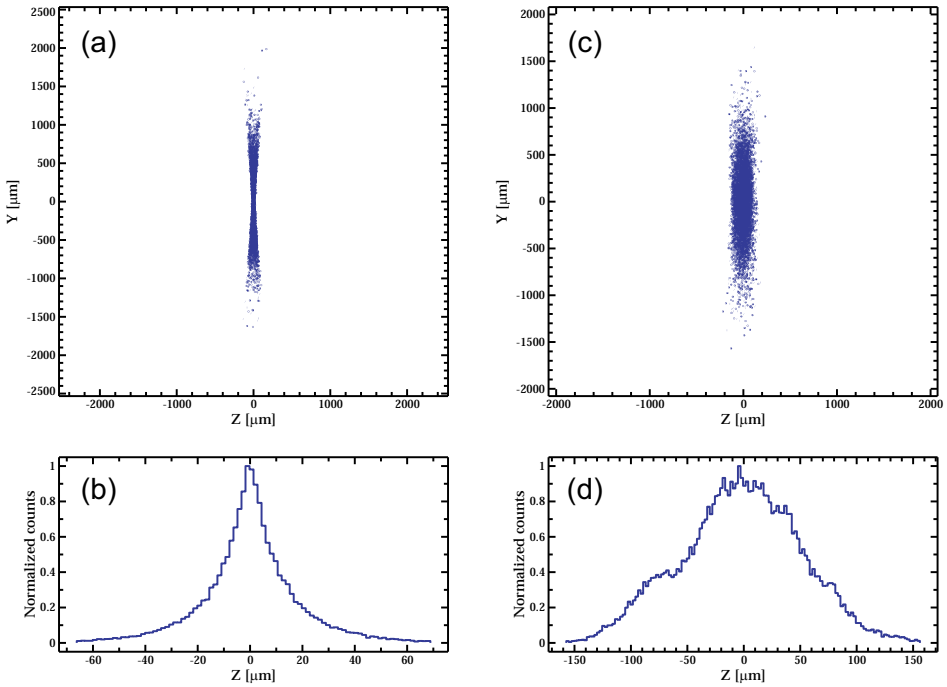

Figure 3. Ray trace results of an on-axis point source at the focus of a sub-apertured Wolter I telescope of IXO dimensions and 4.6 arcsec PSF (HPD), showing the detrimental effects of decenter-like misalignments. (a) 2-D PSF from a mirror without any decenter errors, sub-apertured to 2×10 deg. (b) 1-D LSF of (a) projected onto the dispersion axis. (c) 2-D PSF from a mirror with 2 arcsec decenter contribution, sub-apertured to 2×10 deg. (d) 1-D LSF of (c) projected onto the dispersion axis. Note the different lateral scales for (b) and (d).

3. SPECTRAL RESOLUTION, SUB-APERTURING, AND COMPOSITION OF THE MIRROR PSF

The resolving power of a grating spectrometer is given by the ratio $R = E/\Delta E$ or $\lambda/\Delta\lambda$, where E is the energy of a given photon and ΔE is the FWHM of an unresolved spectral line. For telescopes similar to IXO R is, to first order, proportional to the grating dispersion angle and the dispersion distance or Rowland spacing (distance from gratings to spectral focus), and inversely proportional to the width of the line spread function (LSF), which is the 2-D mirror point-spread function (PSF) projected onto the grating dispersion axis. The CATGS places the gratings at maximum distance from focus and utilizes higher diffraction orders via blazing to increase dispersion angles. If the CATGS were to utilize the full telescope aperture its resolution would be limited to $R \sim 2100$. While this would be a significant improvement over previous missions - especially in combination with the much larger effective area - it does not meet the goal of $R = 3000$. However, in order to meet the effective area requirement only a fraction of the telescope aperture needs to be covered by gratings. Due to the high diffraction efficiency of the CAT gratings it suffices to cover two azimuthal sectors of only 30° each. (Radial coverage extends only over roughly the outer two thirds of mirror radii, leaving the innermost mirrors that supply the bulk of the effective area for higher energies unobstructed and available for the focal plane instruments.) This azimuthal sub-aperturing leads to the welcome effect of narrowing the PSF utilized by the gratings, and therefore reducing the width of the LSF and boosting spectral resolution.

A strong *caveat* needs to be stated here. The extend to which the LSF is narrowed through sub-aperturing depends on the detailed makeup of the mirror PSF, or on the relative contributions of mirror scatter, figure errors, and misalignments to the PSF. Sub-aperturing works so well primarily for grazing-incidence optics such as Wolter I x-ray mirrors because scattering from roughness and high-to-mid-spatial-frequency figure errors is predominantly in the plane of reflection and much narrower in the out-of-plane direction.[9] By aligning the grating dispersion axis with the mirror out-of-plane direction one can take advantage of this narrow out-of-plane

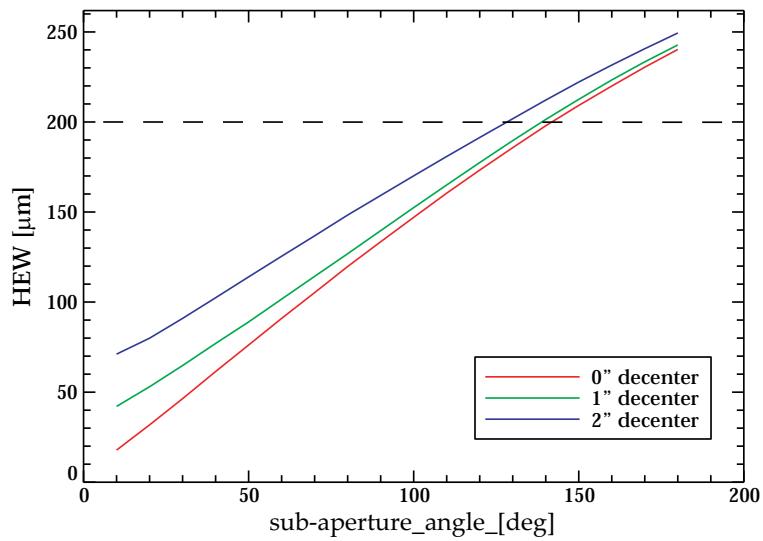

Figure 4. Ray trace results of the HEW of the 1-D LSF as a function of sub-aperture angle obtained from the projection of a sub-apertured 2-D mirror PSF with 4.6 arcsec HPD. Higher decenter contributions to the mirror PSF negate the resolution-improving effects of sub-aperturing. The dashed line shows the acceptable LSF HEW to achieve $R = 3000$ for a grating array placed 19.7 m from focus. Our current design uses a sub-aperture angle of 30°.

scattering. In this case sub-aperturing could theoretically be used to shrink the LSF to near zero (reducing the effective area to near zero at the same time). However, the IXO mirrors are comprised of a large number of mirror shell or plate pairs, and misalignments between them will contribute to the required 5 arcsec imaging PSF. For example it is easy to see that small lateral offsets from nominal mirror positions (normal to the optical axis) will "smear out" a narrow sub-apertured LSF and therefore limit the effect of sub-aperturing.

We have performed ray-trace studies to investigate the effects of sub-aperturing and differences in contributors to the mirror PSF, as well as grating-related effects. Our model is based on the MARX simulator for Chandra.[10] Mirrors initially consist of ideal Wolter I non-segmented shell pairs with parameters from the current NASA GSFC slumped glass[11] model. A number of error terms can be added into the model independently. Mirror scatter and figure errors are simulated as Gaussian random variations in the mirror surface normal upon reflection ("scatter"). Misalignments are simulated as Gaussian random rotations and displacements of individual shells, with displacements broken down into "defocus" (displacement along the optical axis) and "decenter" (displacement in the plane normal to the optical axis). Rotations are around random axes normal to the optical axis. The Gaussian widths for all four terms can be varied independently to achieve a desired mirror PSF.

As an example we modeled the mirror PSF as a function of sub-aperture angle for three cases. For all three cases the full aperture PSF was adjusted to 4.6 arcsec (HPD), leaving some room for observatory-level and aspect reconstruction effects. In the first case the 4.6 arcsec PSF was generated from scatter only, while the other cases had one and two arcsec contributions, respectively, from decenter, with the rest due to scatter. As shown in Figures 3 and 4 the resulting half energy width (HEW) of the LSF at focus is lowest for the scatter-only case and increases with increasing decenter contributions. This effect only describes the change in LSF at focus due to sub-aperturing and is independent of grating and spectrometer design. Two arcsec of decenter seems to be in rough agreement with those imaging error budget terms for the NASA slumped glass model that are not amenable to sub-aperturing, such as decenter terms. Fortunately, in the case of the CATGS placing the gratings far from focus allows us to achieve $R = 3000$ with a LSF HEW as large as ~ 200 μm. With a sub-aperture angle of 30° we therefore have enough room left to accommodate grating and observatory level terms or even higher decenter-like contributions from the mirrors. Alternatively, if non-mirror error terms can be held small enough there is potential to increase the resolution significantly above the requirement. In contrast, moving the gratings from their maximum distance closer to focus would require a proportional reduction in the LSF to maintain the required resolution, eventually putting additional requirements on the composition of the already challenging to

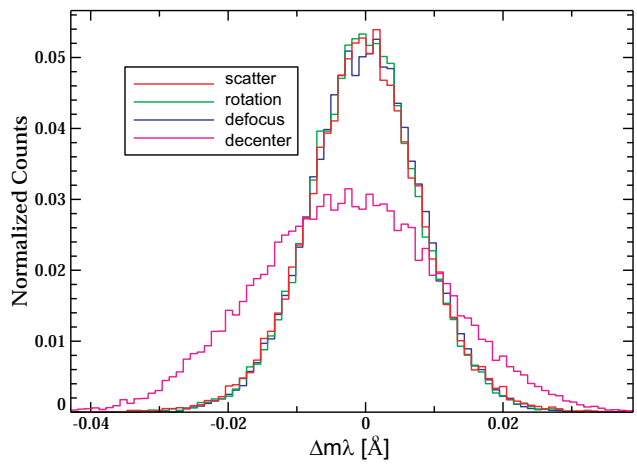

Figure 5. Ray trace results of the 1-D LSF on the CATGS camera obtained from the projection of a $2 \times 30°$ sub-apertured and diffracted 2-D mirror PSF with 4.6 arcsec HPD as a function of shift in $m\lambda$ from a nominal spectral line (diffraction order $m = 3$, wavelength $\lambda = 35$ Å). See text for details.

achieve mirror PSF.

We also inserted CAT grating arrays according to the above optical design into the model. The arrays consisted of flat 60×60 mm^2 facets, arranged in two juxtaposed 30° sectors. We further chose for now to represent the dominant grating related error term as a relative variation in grating period $\Delta p/p = 60$ ppm. Four different mirror models were then investigated, where the 4.6 arcsec mirror PSF was generated from a single error term (scatter, decenter, rotation/tilts, defocus). Except for the decenter case all models give similar results with FWHM corresponding to $R \sim 5500 - 5800$ (see Fig. 5). The decenter case gives $R \sim 3370$ (FWHM), leaving hardly any room for additional resolution degrading effects. Again this demonstrates that decenter-like terms in the telescope imaging error budget have the potential to negate improvements in spectral resolution from sub-aperturing. On the other hand our ray trace studies show that we can safely expect to achieve the required resolution and that we can probably exceed it by a significant amount.

4. CONFIGURATION STUDIES

Detailed CATGS configuration studies have been preformed previously in support of the IXO submission to the Astro2010 Astronomy and Astrophysics Decadal Survey[12] and demonstrated the CATGS to be a viable instrument that will meet the soft x-ray science requirements with modest use of spacecraft resources.[5] These studies were based on a NASA spacecraft concept and the GSFC segmented slumped glass FMA.

4.1 Adaptation to Silicon Pore Optics

In support of the ongoing ESA Cosmic Vision planning process we adapted our instrument design to a silicon pore optic (SPO) FMA[13] and ESA spacecraft resource concept. While slumped glass and SPO FMA models differ in dimensions, structural layout, and distribution of effective area, we maintained the basic grating array design of two opposing grating array structures (GAS) that cover $\sim 30°$ each in azimuth. The layout of the GAS was modified to place most of its structure in locations that do not contribute to the SPO effective area. Only some of the thin grating facet frames lead to additional blockage on the order of 1.6% of the area covered by gratings. As in the case of the slumped glass FMA, radial coverage begins at the outermost mirror radius and ends towards smaller radii as soon as the effective area requirement is met. The resulting effective area as a function of energy is shown in Fig. 6. Meeting the requirement at the lowest energy results in effective areas up to > 1800 cm^2.

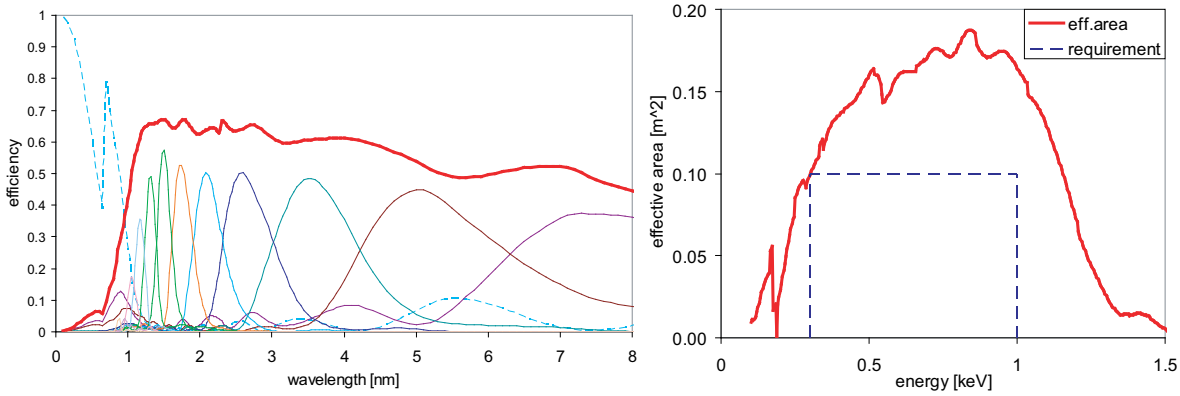

Figure 6. Left: Theoretical diffraction efficiency of a 200 nm-period silicon CAT grating. The red line shows the sum of diffraction efficiencies from orders 1-12, and the dashed line shows 0th order transmission, which contributes to effective area at the telescope focus. Right: Effective area of a SPO-compatible CATGS as a function of energy, taking into account telescope coverage, effective mirror area as a function of energy and mirror radius, blockage from grating array structure and support meshes, grating diffraction efficiencies, CCD filter transmission, CCD quantum efficiencies, and CCD array size. The effective area at 0.3 keV dictates the grating array size. The effective area exceeds the requirement by far for most of the energy band.

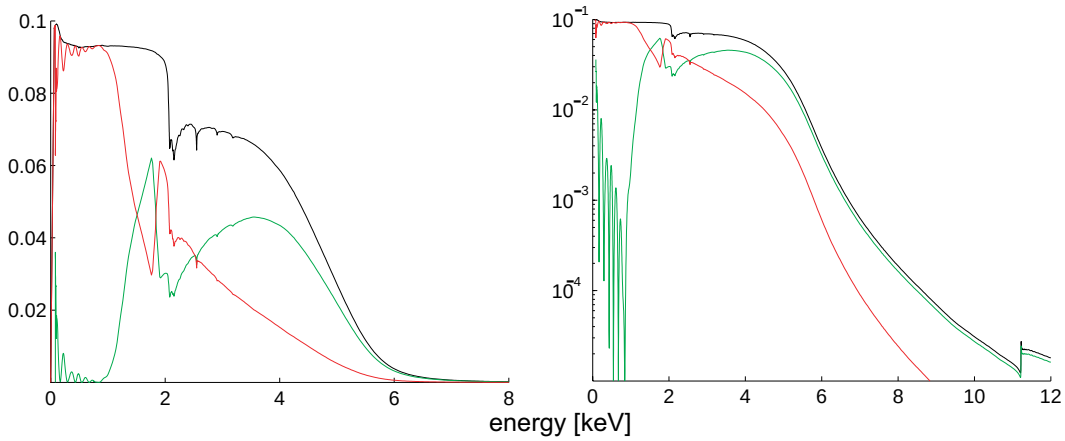

Figure 7. Effect of gratings on effective area at focus as a function of x-ray energy (slumped glass FMA). Left: Linear plot. Right: Semi-log plot. Black curve: Mirror effective area fraction covered by grating arrays. Green curve: Mirror effective area fraction that is transmitted through the grating arrays to the telescope focus. Red curve: Mirror effective area fraction that is removed from effective area at focus (difference between black and green curves - includes x rays that are diffracted onto the CATGS camera and x rays that are lost through structural blockage).

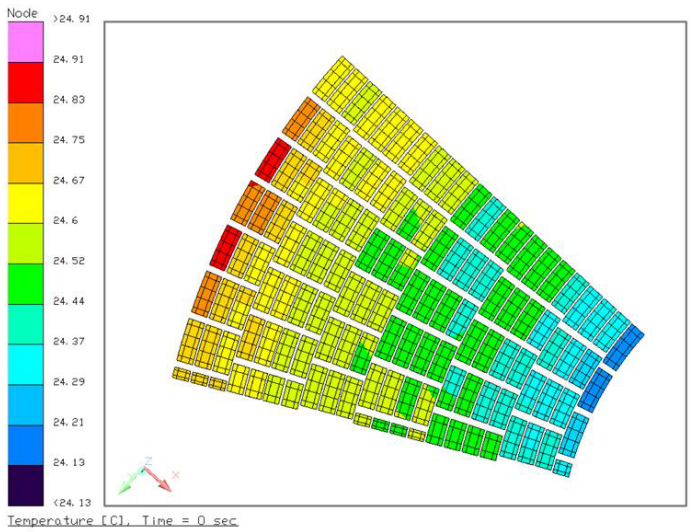

Figure 8. Typical temperature distribution across an SPO compatible grating array. Note that most grating facet temperatures are within $\sim 0.3°$C of each other.

4.2 Mass and power

The total mass for a mechanically acceptable pair of SPO-compatible GAS, including all the gratings, is estimated to be only 9.6 kg, with further light-weighting possible. The bulk of the instrument mass ($\sim$ 88.7 kg) lies in the camera assembly (shielding, focal plane, etc.) and associated hardware (focus actuators and flexures, baffles, harnesses, etc.), as well as readout and processing electronics for the linear 32-CCD array. The grating array will not require any electric power. Peak instrument power on the detector end is estimated at 113.6 W. The readout camera is expected to be "always on", thereby maximizing scientific yield in the area of high-resolution soft x-ray spectroscopy even during observations that are dedicated to any of the focal plane instruments. At the same time the presence of the gratings has minimal impact on the effective area at the telescope focus, especially at higher energies, as shown in Fig. 7.

4.3 Thermal modeling

Earlier studies of a very simple thermal GAS model for the slumped glass FMA indicated that temperature non-uniformity that could lead to variations in grating period is not expected to have a large effect on the spectral resolution of the CATGS. In order to confirm this conclusion we have recently performed a detailed thermal study of a CAD model of the SPO compatible version of the grating array that is fully populated with grating facets. Due to a lack of a thermal model for the SPO FMA we placed the grating array into the thermal model for the NASA spacecraft and FMA version. While electromagnetic modeling of the thermal emissivity of CAT grating membranes lead to nominal values around 0.1, a parametric study was done where we varied emissivity and transmissivity over a large range independently for both sides of the membranes. In the nominal case the maximum temperature difference over a grating sector was found to be 1.1°C, and the largest difference found over the whole range of parameters was 2.3°C. However, the maximum temperature difference is dominated by a few outliers, and the facet temperature distribution can be fit well to Gaussians with sigmas in the range of $0.15 - 0.2°$C. For our silicon grating membranes we expect a change in grating period of 0.52 ppm per 0.2°C change in temperature, which is about two orders of magnitude smaller than grating associated terms assumed in our ray-traces. The maximum temperature difference within the standoffs that connect the grating arrays to the FMA was found to be about 3°C. Such small temperature gradients have no appreciable effect on the stability of the grating array alignment. Furthermore we found that the heat load of a grating sector onto the mirrors next to it does not exceed 1.5 W in the worst case (the gratings transmit heat from the warmer metering structure to the slightly colder mirrors). Such a small additional load is not expected to have a significant impact on

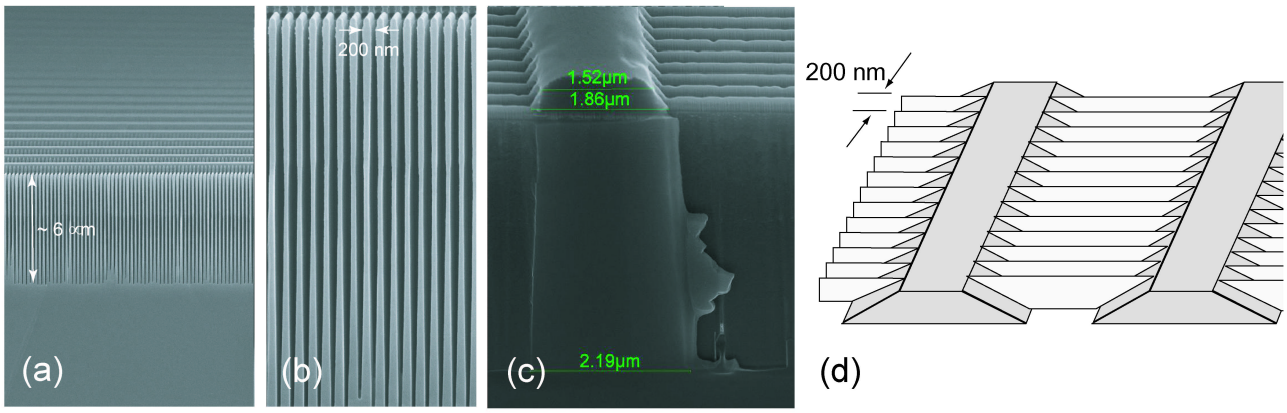

Figure 9. Scanning electron micrographs of cleaved cross sections of deep-reactive-ion-etched silicon gratings before mask removal. (a) Cross section through 6 μm deep 200 nm-period grating bars. Many rows of cross supports - running parallel to the cleave - can be seen at the top. (b) Blow-up of (a). The "bowing" of the sidewalls will be eliminated through a short KOH "polish". (c) Cross section through support mesh bar, showing the nearly vertical support bar sidewalls. (d) Schematic of previously fabricated CAT gratings, showing the widening of the (grey) support bars with increasing KOH etch depth. This widening is now strongly reduced, as can be seen from (c).

the mirror thermal control. From our thermal studies it thus appears that temperature gradients in the grating arrays are of no major concern and that active temperature control of the gratings is not needed.

5. FABRICATION OF 200 NM-PERIOD CAT GRATINGS

CAT gratings that are designed to meet IXO requirements essentially are comprised of periodic arrays of free-standing, parallel, 30-40 nm thin, and $\sim 6\mu$m deep silicon CAT grating bars or nanomirrors.[6] The nanomirrors are inclined at a small grazing angle (1.5°) relative to the incident x rays. For soft x rays this angle is below the critical angle of total external reflection, leading to effective blazing at angles around twice the graze angle relative to the incident x rays. Grating diffraction orders that lie within this blaze envelope are strongly enhanced and provide high diffraction efficiency. Peak efficiencies of above 50% have been observed experimentally.[5,6] The fabrication process for 200 nm-period gratings has been described in detail elsewhere.[14–16] The nanomirrors are held at their sides by a coarse period support mesh that is monolithically integrated into the grating membrane. In all our gratings fabricated so far the high aspect ratio of the nanomirrors (height/width ~ 150) was achieved through anisotropic wet etching of a patterned <110> silicon-on-insulator (SOI) wafer device layer in KOH. While such an etch can provide the required high aspect ratio and almost atomically smooth {111} silicon mirror surfaces, it also stops on the strongly inclined {111} sidewalls of the support mesh and leads to increasing loss of nanomirror surface with increasing etch depth (see Fig. 9).

An alternative approach is to first etch the nanomirror and support mesh mask pattern vertically $\sim 6\mu$m deep into the SOI device layer with a crystal-lattice-independent etch. If that etch can not deliver the required nanomirror surface smoothness the first etch can be followed by a short KOH "polishing" step.[16] Again, achieving such high aspect ratios for such a small grating period without destroying the thin mirrors is a challenge. However, as shown in Fig. 9 we have recently performed successful demonstrations of a deep reactive ion etch (DRIE) that meets our goals for the nanomirrors without significant broadening of the support mesh bars.[17] This fabrication breakthrough will allow us to optimize the structural design of the support mesh and to meet the goal of high-throughput CAT gratings with no more than 10% relative efficiency loss from the support mesh.

6. DISCUSSION, SUMMARY, AND OUTLOOK

The critical-angle transmission grating spectrometer presented in this and previous publications will provide an unprecedented combination of high resolving power ($R \sim 5000$) and effective area (> 1000 cm^2) for soft x-ray

spectroscopy on board IXO. Detailed ray trace studies of the optical design with realistic mirror models show that there is room in the resolution error budget that allows for a trade between resolution and effective area by increasing coverage in the azimuthal direction and/or radially inwards. For example, the effective area could easily be doubled by doubling the sub-aperture angle of the lightweight grating arrays without violating the resolution requirement (see Fig. 5). In this case the effective area would exceed 3000 cm^2 for most of the 0.3 to 1.0 keV band. We invite the soft x-ray spectroscopy astrophysics community to weigh in on this trade.

With the recent SPO focused CATGS studies we now have identified instrument configurations that are compatible with both the NASA and ESA led spacecraft and optics concepts and technologies.

Our CAT grating fabrication efforts are on schedule with regards to our technology and instrument development plans which are compatible with an IXO launch date of early 2021. With the fabrication developments described above we expect to make appropriate progress on our near-term goals of increased grating throughput and size.

ACKNOWLEDGMENTS

We gratefully acknowledge technical support from R. C. Fleming (Space Nanotechnology Laboratory), as well as facilities support from the Nanostructures Laboratory and the Microsystems Technology Laboratories (all at MIT), as well as the Lurie Nanofabrication Facility at the University of Michigan. We also thank P. Reid, J. Lasco and S. Jordan for helpful discussions. Various parts of this work were supported by NASA grants NNX07AG98G, NNX08AI62G and NNX09AE82A.

REFERENCES

[1] C. R. Canizares *et al.*, "The Chandra high-energy transmission grating: Design, fabrication, ground calibration, and 5 years in flight," *PASP* **117**, 1144-1171 (2005).

[2] See for example http://ixo.gsfc.nasa.gov/.

[3] See for example http://space.mit.edu/home/nss/cat_science.html

[4] K. Flanagan *et al.*, "Spectrometer concept and design for x-ray astronomy using a blazed transmission grating," *Proc. SPIE* **6688**, 66880Y (2007).

[5] R. K. Heilmann *et al.*, "Development of a Critical-Angle Transmission Grating Spectrometer for the International X-Ray Observatory," *Proc. SPIE* **7437**, 74370G (2009).

[6] R. K. Heilmann, M. Ahn, E. M. Gullikson, and M. L. Schattenburg, "Blazed high-efficiency x-ray diffraction via transmission through arrays of nanometer-scale mirrors," *Opt. Express* **16**, 8658-8669 (2008).

[7] R. K. Heilmann, M. Ahn, and M. L. Schattenburg, "Fabrication and Performance of Blazed Transmission Gratings for X-Ray Astronomy," *Proc. SPIE* **7011**, 701106 (2008).

[8] J. W. den Herder *et al.*, "The reflection grating spectrometer on board XMM-Newton," *Astr. & Astroph.* **365**, L7-L17 (2001).

[9] W. C. Cash Jr., "X-ray optics 2: A technique for high-resolution spectroscopy," *Appl. Opt.* **30**, 1749-1759 (1991).

[10] M. W. Wise, D. P. Huenemoerder, and J. E. Davis, "Simulated AXAF observations with MARX," *Astronomical Society of the Pacific Conference Series* **125**, 477-480 (1997).

[11] W. W. Zhang *et al.*, "Mirror technology development for the International X-ray Observatory mission," *Proc. SPIE* **7437**, 74370Q (2009).

[12] See for example http://ixo.gsfc.nasa.gov/resources/0209 Decadal WhitePapers.html.

[13] K. Wallace *et al.*, "Silicon pore optics development," *Proc. SPIE* **7437**, 74370T (2009).

[14] M. Ahn, R. K. Heilmann, and M. L. Schattenburg, "Fabrication of ultrahigh aspect ratio freestanding gratings on silicon-on-insulator wafers," *J. Vac. Sci. Technol. B* **25**, 2593-2597 (2007).

[15] M. Ahn, R. K. Heilmann, and M. L. Schattenburg, "Fabrication of 200 nm-period blazed transmission gratings on silicon-on-insulator wafers," *J. Vac. Sci. Technol. B* **26**, 2179-2182 (2008).

[16] M. Ahn, "Fabrication of Critical-Angle Transmission gratings for high efficiency x-ray spectroscopy," Ph.D. thesis, Department of Mechanical Engineering, Massachusetts Institute of Technology (2009).

[17] P. Mukherjee, A. Bruccoleri, R. K. Heilmann, M. L. Schattenburg, A. F. Kaplan, and L. J. Guo, "Plasma etch fabrication of 60:1 aspect ratio silicon nanogratings on 200 nm pitch," submitted to *J. Vac. Sci. Technol. B*.